A Model for Membrane Patchiness: Lateral Diffusion in the Presence of Barriers and Vesicle Traffic

Levi A. Gheber and Michael Edidin
Department of Biology, Johns Hopkins University, Baltimore, Maryland 21218 USA

ABSTRACT Patches (lateral heterogeneities) of cell surface membrane proteins and lipids have been imaged by a number of different microscopy techniques. This patchiness has been taken as evidence for the organization of membranes into domains whose composition differs from the average for the entire membrane. However, the mechanism and specificity of patch formation are not understood. Here we show how vesicle traffic to and from a cell surface membrane can create patches of molecules of the size observed experimentally. Our computer model takes into account lateral diffusion, barriers to lateral diffusion, and vesicle traffic to and from the plasma membrane. Neither barriers nor vesicle traffic alone create and maintain patches. Only the combination of these produces a dynamic but persistent patchiness of membrane proteins and lipids.

INTRODUCTION

The fluid mosaic model of cell membrane architecture (Singer and Nicolson, 1971) emphasizes the autonomy and diffusional mobility of membrane lipids and proteins and the consequent lack of lateral organization of bilayer membranes. In contrast, an alternative model suggests that membranes are organized into domains, local concentrations of membrane proteins and lipids, which may be hundreds of nanometers in diameter (Jain and White, 1977). Experimental evidence has accumulated that cell membranes, particularly cell surface membranes, are indeed laterally heterogeneous on scales that appear to range from tens of nanometers to a few microns. These heterogeneities are commonly referred to as "microdomains," to contrast them with the membrane macrodomains, the functionally differentiated surfaces of epithelial and other morphologically polarized cells. The organization of membranes into microdomains is biologically interesting because membrane microdomains could strongly affect membrane functions by concentrating interacting species in domains (Peters, 1988) or by affecting the percolation of interacting molecules between domains (Thompson et al., 1995; Piknova et al., 1996).

Different approaches have been used to characterize protein-rich and lipid-rich domains (Edidin, 1992; Kusumi and Sako, 1996; Edidin, 1997). However, all characterizations and definitions of domains depend on the experimental method used to detect lateral heterogeneities. Despite this, most of the methods for detecting proteins in patches seem to report membrane microdomains some hundreds of nanometers in diameter. Fluorescence photobleaching recovery (FPR) measurements showed that lateral diffusion of membrane proteins is restricted on a scale of hundreds of nanometers. The apparent mobile fraction of labeled protein decreased with increasing area bleached (Yechiel and Edidin, 1987). This result is not expected if lateral diffusion is bounded only by the total surface area of a cell, because even the largest areas bleached were $<1\%$ of this area. A laser optical trap (LOT) experiment showed that membrane proteins labeled by antibody-coated beads and dragged across the cell surface with an optical trap met obstacles to their mobility on an average of every 1 μm at 22°C and every 3–4 μm at 34°C (Edidin et al., 1991). Later experiments indicated that the frequency with which the particle escaped the trap depended upon the trapping force, but still scaled the spatial frequency of the obstacles to hundreds of nanometers (Sako and Kusumi, 1995). FPR and LOT experiments also showed that the obstacles to lateral mobility, implicated in domain creation, were not in the membrane proper but in the cell cytoplasm (Edidin et al., 1991; Edidin and Stroynowski, 1991; Edidin et al., 1994).

An important connection was made between spatial frequency of barriers to lateral mobility and membrane domains when methods evolved for the analysis of single particle tracking (SPT) data. An SPT experiment follows the Brownian motion of membrane proteins and lipids in terms of the change in position of antibody-coated beads bound to the molecules of interest. Although in light microscopy the beads, usually 50-nm diameter, appear as dots of several hundred nanometers in diameter, the change in position of the centroid of a bead can be tracked with nanometer precision (Schnapp et al., 1988 and other references summarized in Saxton and Jacobson, 1997). The particle tracks derived from sequential video frames of a labeled cell thus yield information about the lateral diffusion, the random walk, of the bead-labeled molecules. It was evident from the very first that analysis of the particle tracks could also indicate whether lateral motion was driven (by flow) or a hindered or bounded random walk, rather than unhindered lateral diffusion. A bounded random walk is

Received for publication 9 March 1999 and in final form 1 September 1999.

Address reprint requests to Dr. Michael Edidin, Dept. of Biology, Johns Hopkins University, Charles and 34th Sts., Baltimore, MD 21218-2685. Tel.: 410-516-7294; Fax: 410-516-5213; E-mail: EDIDIN@JHU.EDU

0006-3495/99/12/3163/13 $2.00

evidence for confinement of the labeled molecules in a corral or domain. Several innovative approaches to the statistics of random walks give reasonably accurate characterization of the frequency of hindered lateral diffusion. These approaches and the entire field of SPT are reviewed in an excellent review by Saxton and Jacobson (1997). The data reviewed there not only give good evidence for confinement of membrane proteins to domains, they also include data on the dwell time of particles within a domain, giving values for the frequency of opening of barriers to unhindered lateral mobility. Data taken at video rates yield typical domain diameters of 200–500 nm and dwell times of ~7 s, though smaller domains and shorter dwell times have been measured in erythrocytes (Tomishige and Kusumi, 1998). The implication is that membrane proteins may be confined on a number of time and distance scales. Indeed, it has been proposed that diffusing molecules encounter potential traps, arresting them on a wide range of energy (and hence time and distance) scales (Feder et al., 1996).

One type of lipid domain has also received a good deal of attention: so-called detergent-insoluble rafts, membrane fractions insoluble in cold Triton X-100, which appear to concentrate glycosylphosphatidylinositol- (GPI-) anchored proteins, glycolipids, cholesterol, and signaling kinases (Simons and Ikonen, 1997). Detergent extraction does not itself define the size of these domains (assuming that they are not artifacts of extraction). Estimates of their size range from hundreds of nanometers, based on SPT of GPI-anchored proteins (Sheets et al., 1997; Pralle et al., 1999) to a few nanometers (Scheiffele et al., 1997). If the rafts do occur in native membranes (Stauffer and Meyer, 1997), they may form due to lipid/lipid interactions (for example see Brown and London, 1997) or may be driven to form by proteins in, or adherent to, the membrane bilayer (see review in Edidin, 1997; also Denisov et al., 1998; Sabra and Mouritsen, 1998).

High-resolution imaging of the cell surface has been used in an attempt to visualize the membrane domains implied by other techniques. Fluorescence microscopy can resolve large-scale heterogeneities in both protein and lipid, particularly after aggregation of membrane receptor proteins (for example Holowka and Baird, 1996; Monks et al., 1998). Both electron microscopy and scanning probe microscopy have imaged cell surface heterogeneities of membrane proteins on a scale of hundreds of nanometers. Damjanovich and co-workers have used atomic force microscopy and electron microscopy to characterize patches of proteins in cell surface membranes (Damjanovich et al., 1997). We have used near-field scanning optical microscopy (NSOM; Betzig et al., 1991; Betzig and Trautman, 1992) to image patches of proteins and lipids, segregated from one-another, in fibroblast cell surface membranes (Hwang et al., 1998; Gheber et al., 1998).

The sizes of patches in high-resolution images of the cell surface are consistent with the sizes of membrane domains implied by FPR, SPT, and LOT experiments. However, the persistence of these patches at steady state is not consistent with a membrane in which proteins and lipids are free to diffuse, and in which barriers to this lateral diffusion open every few seconds. If patches persist, they must either be stabilized by specific molecular interactions or they must reflect some other aspect of membrane physiology at steady state. One such aspect is vesicle traffic to and from the cell surface (Steinman et al., 1983). We have made a quantitative model of the cell surface that includes random walks, dynamic barriers to lateral diffusion, and vesicle traffic. Analyzing this model, we find that vesicle traffic, together with dynamic barriers to lateral diffusion, can create and maintain patches on a scale of hundreds of nanometers, apparent membrane domains. The barrier spacing scales the size of the patches. Vesicle traffic, the delivery and removal of membrane components, determines the persistence of the population of patches and their concentration relative to the average for the entire membrane. Under these conditions, the average number and size of patches is maintained. However, individual patches are short-lived; because the barriers to lateral mobility open transiently, component molecules of the patches diffuse away from the site of delivery. If the barriers are removed, or if vesicle traffic is stopped, the entire population of membrane patches decays to one in which mobile proteins and lipids are uniformly distributed.

METHODS

The plasma membrane was simulated as an array of 128 × 128 pixels. Each array entry (pixel) could be occupied by more than one particle; this accounts for the finite "resolution" of the observer. Diffusion of the particles was simulated as a two-dimensional (2D) random walk, and each particle was moved independently according to the algorithm described below and in Fig. 1. We defined a network of barriers as an array of squares, 8 × 8 pixels in size, superimposed on the pixel array that represents the plasma membrane. The barriers have zero "width"; they are just fences between pixels. Each domain in which free diffusion is allowed is 8 × 8 pixels in size and is enclosed by barriers on all four sides. For example, the pixel at $x = 7$, $y = 5$ is the rightmost one in the lower left corner compartment ($x = 0$ is the leftmost) and the pixel at $x = 8$, $y = 5$ is the leftmost one in the second compartment, to the right of the previous one. In order to jump from $x = 7$, $y = 5$ to $x = 8$, $y = 5$, a particle has to cross a barrier. A characteristic time for hopping across a barrier is defined T_h. If a diffusing particle chooses to make a step in a direction that takes it across a barrier, it has a probability $1/T_h$ of crossing the barrier and a probability $1 - 1/T_h$ of being confined by the barrier. The barriers can be enabled or disabled. Characteristic times for delivering particles to or removing them from the simulated plasma membrane were defined as T_a and T_d, respectively. The number of particles delivered or removed by a vesicle was also defined as N_a and N_d. In order to conserve the total number of particles in the membrane, $T_a = T_d$ and $N_a = N_d$. For vesicle traffic one of the 256 compartments was randomly chosen. To simulate delivery of particles to the surface by a vesicle, exocytosis, N_a particles were added to the chosen compartment at random positions. To simulate removal of particles from the surface by endocytosis, N_d particles were removed from the chosen compartment. If there were less than N_d particles present in the specific compartment, all the particles were removed. Delivery and intake did not occur simultaneously, but at different time points.

The algorithm

The algorithm is described schematically in Fig. 1. The pixels in the array simulating the membrane are assigned values by a random generator

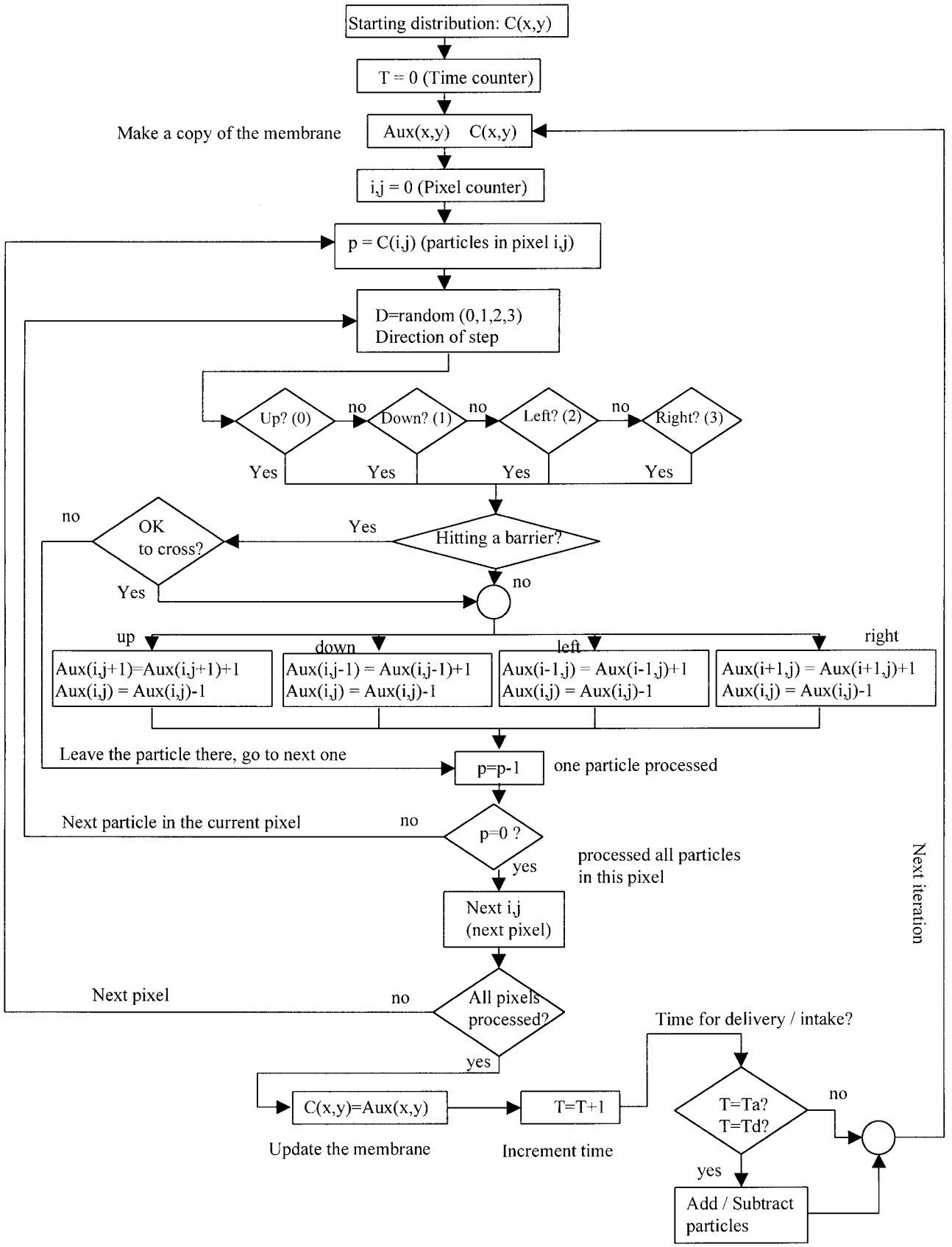

FIGURE 1 Schematic presentation of the algorithm used for the simulations. A detailed description of each step is given in the text.

according to a chosen distribution. The value of each pixel represents the number of particles in that position. A copy of the array is made that will contain the new values of the pixels at the end of one iteration. Each pixel is checked for the number of particles it contains and then each particle is assigned one of four jumping directions (up, down, left, right). The algorithm checks whether the chosen direction will require the particle to cross a barrier (when barriers are enabled). If the chosen direction does not require crossing a barrier, the algorithm actually performs the jump, as explained below. If, in the chosen direction, the particle will meet a barrier, a decision is taken whether the particle is allowed to cross or not, based on the probability $1/T_h$. If the particle is permitted to cross the barrier, then the actual jump is performed as explained below. If not, the particle is left in place and the next particle in the pixel is processed. A particle is not processed more than once in one iteration, or an error in its timekeeping will be introduced.

Processing multiple particles in a pixel is relatively straightforward. There is no need to "label" the particles, just to add "1" to the adjacent pixel to which the particle jumps, and subtract "1" from the pixel from which it jumped. The counting of particles in the pixel is done on the original "membrane," while the addition and subtraction as above is done on the copy of the membrane. This process is repeated as many times as there are particles in the original pixel (the original array). This way, every particle jumps only once in one iteration. Spherical boundary conditions are imposed such that the opposite edges of the array are continuous with each other. A particle jumping off the boundary of the array is returned to the appropriate pixel at the opposite boundary.

Once all the particles in one pixel have been processed, the next pixel is addressed in the same manner. After all the pixels have been processed the original array is updated with the new numbers of particles in each pixel, and the time is incremented. If the time is up for particles to be added or subtracted to/from the plasma membrane (if trafficking is enabled), the appropriate event is initiated, as explained above.

A simulation with the parameter values as explained in the section "Scaling the Model to Biological Dimensions" takes approximately 1 s for every 0.01 s of the cell life when run on an IBM compatible PC with a 333 MHz Pentium II computer. Therefore, simulating 200 s of the cell life takes over 5 h, and longer simulations, of thousands of seconds, take 24–48 h.

Spatial autocorrelation analysis of patch size

The one dimensional autocorrelation function is defined as

$$g(\zeta) = g(-\zeta) \approx \int f(x) f(x+\zeta) dx$$

Here $f(x)$ is the function whose autocorrelation is calculated; ζ is a value by which the function $f(x)$ is shifted, termed "the lag"; and $g(\zeta)$ is the autocorrelation function. It is a symmetrical function of the lag and has several interesting properties, as described below and in Hwang et al., 1998 and references therein. Briefly, the function is multiplied by a shifted (by ζ) copy of itself, resulting in a new function, which is then integrated over the whole space of definition, resulting in a value for the particular ζ. The operation is repeated for other values of ζ, ultimately yielding all the values of the function $g(\zeta)$. In the discrete case, the autocorrelation takes the form

$$g_L = g_{-L} \approx \sum_{i=0}^{N-L-1} x_i x_{i+L}$$

where L is the lag, x_i are the discrete values of the function for which the autocorrelation is calculated, and N is the total number of x values. Note that g_0 is proportional to $\Sigma_{k=0}^{N} x_k^2$. In our two-dimensional discrete case:

$$g_{K,L} \approx \sum_{i,j} x_{i,j}\, x_{i+K,j+L}$$

where K, L are the lag in the x and y direction, respectively, and $x_{i,j}$ are the values of the two-dimensional function.

Here $g_{0,0}$ is proportional to the sum of $X_{i,j}^2$ over all entries of X. In other words, its square root is proportional to the RMS of the image. Therefore, $g_{0,0}$ reports on the departure from a flat, uniform distribution and a larger value of $g_{0,0}$ means a more corrugated, more clustered array. We used the autocorrelation value at the origin to compare patchiness of the simulated membrane as it evolved in time.

The autocorrelation function can be fit to a Gaussian function of the form $g = g(0, 0) \exp(-r^2/w^2)$, where r is the distance from the origin and w is the characteristic width of the Gaussian function at $1/e$ of its maximum. The decay rate of the autocorrelation function at the origin is proportional to the average size of patches in the images. By extraction of w, one gets a measure of the characteristic size of the patches. Thus, using the autocorrelation approach, we extract two important values: the degree of patchiness (variance of particle concentration) and the characteristic size of patches. The actual calculation of the 2D autocorrelation function was done using an FFT algorithm (IDL, Research Systems, Inc., Boulder, CO) to calculate the 2D Fourier power spectrum of the images and then using the inverse transform of the power spectrum to obtain the 2D autocorrelation function. This procedure follows from Fourier's convolution theorem.

Modeling free diffusion

To check the validity of the algorithm we simulated free diffusion starting with a Gaussian concentration profile. Four snapshots of the particle concentration, at different times, are shown in Fig. 2. From the diffusion equation it follows that the mean square displacement (MSD) of a freely diffusing particle is linear with time. The MSD of the ensemble of particles was calculated using the autocorrelation of images such as those of Fig. 2. Because the autocorrelation of a Gaussian function is also a Gaussian function, it is fitted to a Gaussian (Fig. 3 *a*). From the fitted function, the width of the Gaussian is extracted and its squared value is plotted versus time (Fig. 3 *b*).

The 2D diffusion coefficient is $D = \frac{1}{4} l^2/\tau$, where l is the step length and τ is the characteristic time to make this step. In our case, $l = 1$ (pixel)

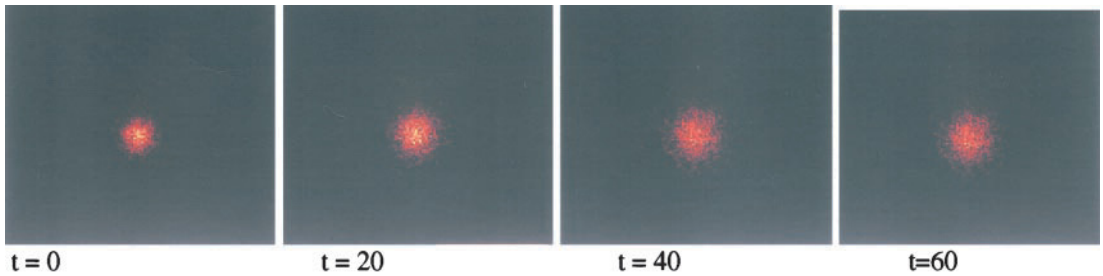

FIGURE 2 Free diffusion, starting with a Gaussian distribution. Four snapshots are taken at four time points (internal time units), as described in the figure. The intensity of each image has been rescaled to cover the entire color scale to allow displaying the spatial distribution (late images are very dark if displayed with the same color scale as early ones). Also see the movie at http://www.bio.jhu.edu/faculty/edidin/pubs/, showing simultaneously the image and its 2D autocorrelation in real time.

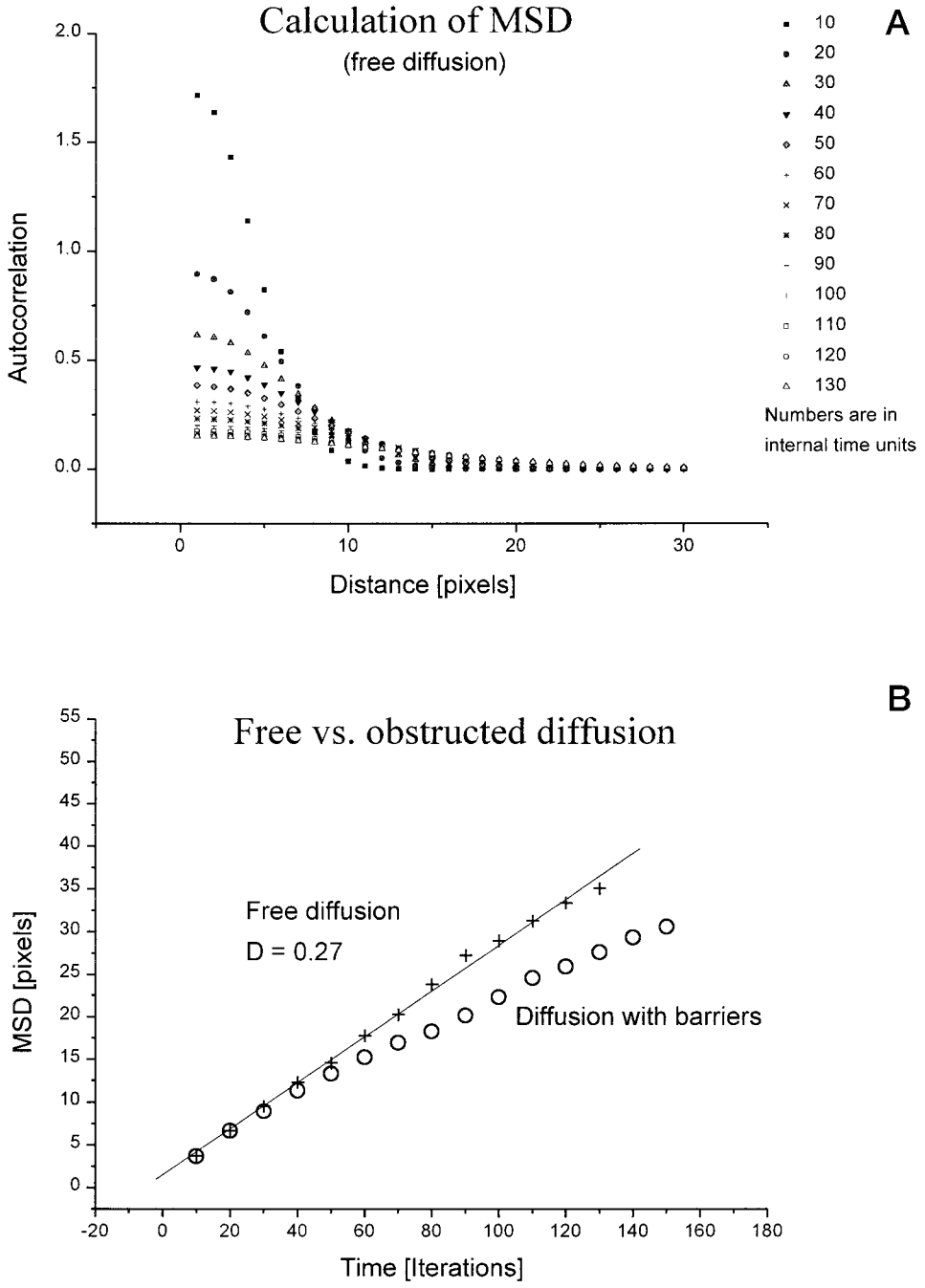

FIGURE 3 Calculation of the diffusion coefficient. (*a*) Profiles of the autocorrelation function at different time points. Each such profile has been fitted to a Gaussian and its width extracted. (*b*) The squared width of the Gaussian, plotted against time, for free diffusion (simulated as in Fig. 2) and for diffusion obstructed by barriers (simulated as in Fig. 4). The slope of the line is expected to be 0.25 for free diffusion in two dimensions; we obtain 0.27, which is satisfactory, given the limitations of our simulation. Note that the first few points (up to ~20 iterations) are identical for free diffusion and for obstructed diffusion. During this time the particles diffuse freely within the compartments and only later, when meeting the barriers, the diffusion is slowed.

and $\tau = 1$ (internal unit time), therefore one expects the slope of the graph for free diffusion in Fig. 3 *b* to be 0.25. We find ~0.27, which is a satisfactory result for the relatively small ensemble and short period of time for which it was followed.

Modeling diffusion with barriers

To check the validity of this model, we started with a Gaussian distribution of particles, in the presence of barriers, with $T_h = 20$. Six snapshots of this model are shown in Fig. 4. Note that at $t = 50$ diffusion is obstructed; the particles occupy a square. This area is actually composed of four 8×8 compartments. As time goes on, the particles slowly diffuse across the barriers, as can be seen in the remaining snapshots. Using the same approach as for free diffusion, the MSD of the particles in this case was also measured and compared with the MSD for free diffusion (Fig. 3 *b*). It can be seen that the first few points coincide in both cases, because the particles diffuse freely, but once the barriers are reached the diffusion rate of the particles is slowed.

RESULTS AND DISCUSSION

Modeling a membrane with lateral diffusion, barriers to lateral diffusion, and vesicle traffic arbitrary parameters

The simulation was started with a random distribution of 64,000 particles (on average 3.9 particles per pixel), without

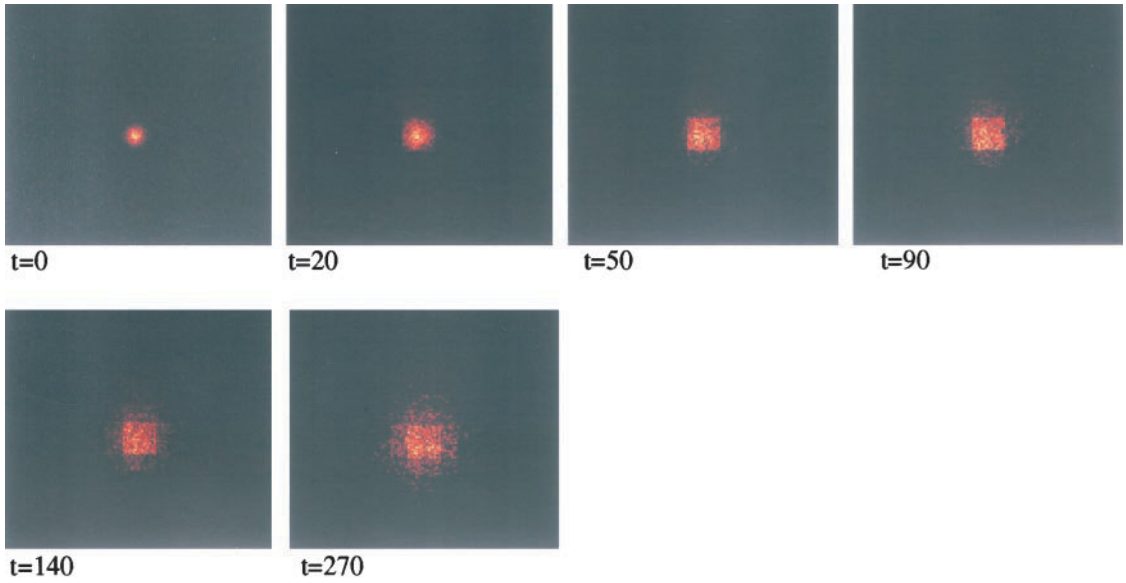

FIGURE 4 Obstructed diffusion, starting with a Gaussian distribution. The center of the initial Gaussian concentration of particles is positioned at the intersection of two perpendicular barriers. Therefore, the particles start diffusing freely into four domains and only later hit the far barriers defining these domains. At $t = 50$ it is obvious from the image that the particles are retained in a square region, which actually consists of four 8×8 adjacent compartments. At later times, the particles escape the barriers and continue diffusing into the next compartments. The snapshots are taken at six time points (internal time units), as described. The intensity of each image has been rescaled to cover the entire gray scale to allow displaying the spatial distribution (late images are very dark if displayed with the same color scale as early ones). Also see the movie at http://www.bio.jhu.edu/faculty/edidin/pubs/, showing simultaneously the image and its 2D autocorrelation in real time.

barriers or delivery/intake. Particles were allowed to diffuse freely for 100 iterations, to $t = 100$. At this point, dynamic barriers were added and lateral diffusion of the system continued for 100 more iterations. At $t = 200$, vesicle traffic, delivery, and intake of particles was started, with $T_a = T_d = 5$ and $T_h = 10$. Traffic continued for 200 iterations, and then, at $t = 400$, vesicle traffic was stopped, but the barriers were not removed. At $t = 600$, after 200 more iterations, the barriers were removed and the system was followed for 60 more iterations. Fig. 5 shows a series of snapshots at different times during the simulation. One row consists of three images which are (from left to right) the image of the simulated membrane, the 2D autocorrelation function of the image, and a 1D section of the 2D autocorrelation function.

The simulation started with a random distribution and free diffusion for 100 iterations. After the addition of barriers (at $t = 100$) and 100 more iterations, the random distribution was maintained, and the autocorrelation function showed no feature (Fig. 5 *a*). Barriers alone are not sufficient to create patchiness of membrane components. Once vesicle traffic, the delivery/intake of particles was started, patchiness appeared quickly (Fig. 5 *b*). It can be seen directly in the images and detected from the autocorrelation function. The amplitude of the autocorrelation at the origin, $g(0, 0)$, constantly increased, reporting on an increasing number of patches (Fig. 5 *c*). Once the delivery/intake was stopped at $t = 400$, the patchy distribution of particles decayed, with a constant decrease in the magnitude of the autocorrelation function, reporting on a decrease in the number of patches (Fig. 5 *d*). Barriers alone cannot maintain a patchy distribution. When the barriers were removed at $t = 600$ the system continued to relax toward a random distribution.

A summary of this simulation is shown in Fig. 6. The lines plot $g(0, 0)$ and the size of the patches as a function of time. The arrows indicate the times when barriers were added or removed, and the times when vesicle traffic, particle delivery/intake, was started and stopped. Besides the features noted in the previous paragraph, we can also see that, once vesicle traffic began, the size of the patches quickly jumped to the predefined size of compartments, ~8 pixels (diagonal = 11.3).

Scaling the model to biological dimensions

The simulation just described above was performed with arbitrary parameters in order to show that nonspecific patches of membrane proteins and lipids, with sizes scaled by barrier spacing, can arise from a combination of diffusion obstructed by the barriers and vesicle traffic. However, even this is not true for some choices of parameters. For example, the relationship between the typical time of diffusion across barriers (T_h) and the rate at which the concentration is modulated by vesicle traffic (T_a, T_d) is a very important factor in determining whether patches will ap-

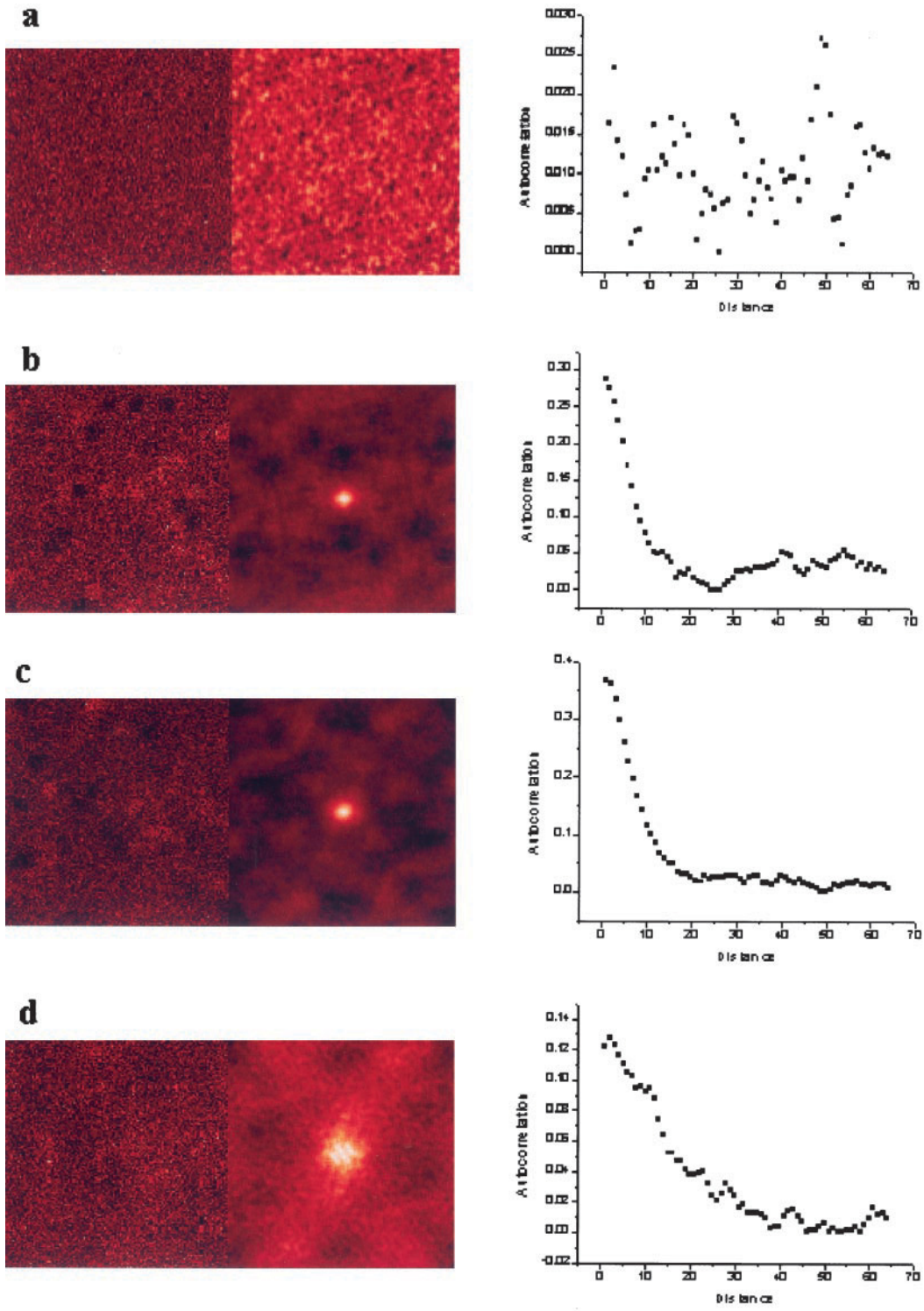

FIGURE 5 Diffusion with barriers, in the presence of vesicle traffic. Each row (*a–d*) consists of (from left to right) the direct image of the simulated membrane, the 2D autocorrelation of the image, and the 1D profile of the 2D autocorrelation. The simulation started with a uniform distribution of particles, diffusing freely for 100 iterations. At $t = 100$ barriers were added and the particles continued to diffuse, now undergoing obstructed diffusion. (*a*) Two hundred iterations after starting the simulation. The distribution is still random and the autocorrelation shows no feature: the barriers alone do not induce clustering. At $t = 200$, the vesicle traffic is started. (*b*) Three hundred iterations after starting the simulation (100 iterations after vesicle traffic started). Bright clusters in the image are due to delivered particles, dark spots are due to intake. The 2D autocorrelation shows a bright spot in the center, representing detection of clusters. (*c*) Three hundred fifty iterations after starting the simulation (150 iterations after starting vesicle traffic, 50 iterations after *b*), the patchiness continues to increase. The vesicle traffic was stopped 400 iterations after starting the simulation (200 iterations after starting the vesicle traffic). (*d*) Five hundred iterations after starting the simulation (100 iterations after stopping the vesicle traffic), the clusters dispersed due to diffusion across the barriers and the lack of a mechanism to maintain the concentration inhomogeneity. Also see the movie at http://www.bio.jhu.edu/faculty/edidin/pubs/, showing simultaneously the image and its 2D autocorrelation in real time.

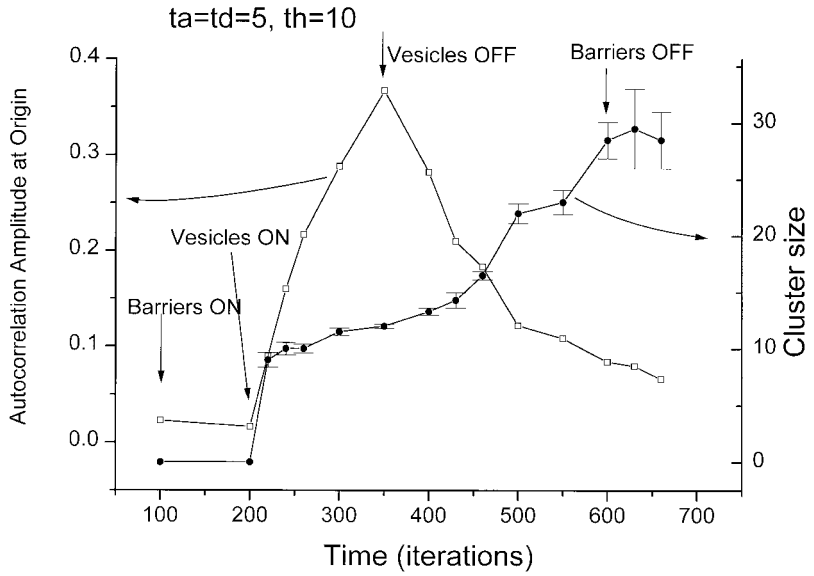

FIGURE 6 Summary of the simulation. The autocorrelation amplitude at the origin (*open squares*) is plotted with values on the left axis; it shows no change as a result of adding barriers, but grows rapidly as vesicle traffic is started after 200 iterations, indicating the evolution of an increasingly clustered membrane. It then falls rapidly when the vesicle traffic is stopped, in the presence of barriers, and continues to fall when the barriers are completely removed. The size of clusters as extracted from the autocorrelation function is plotted (*filled circles*) with values on the right axis. The error bars represent the errors in the width parameter (w, in the expression $G = g(0, 0)\exp(-r^2/w^2)$). A larger error means a less defined cluster size. The expected cluster size is a square of 8×8 pixels, as defined by the initial conditions of the simulation. We note that, due to its averaging properties, the autocorrelation may detect a size that lies between 8 and $\sqrt{2x8^2} \approx 11.3$ (the diagonal of the square domain). The cluster size indeed jumps to 8 as the vesicle traffic is started, and its value raises slowly, with an increasingly good size definition (*small error bars*), up to the point where vesicle traffic is stopped (after 350 iterations). From this point and on, the cluster size grows rapidly while the autocorrelation amplitude decreases, which reports on a homogenization process, a return to random distribution.

pear. If, for instance, diffusion across barriers is very fast compared with the rate of vesicle traffic, ($T_h \ll T_{a,d}$), (lipids are expected to fall into this category) the local concentration change will disperse rapidly, and most of the time the molecules of the membrane will appear to be homogeneously distributed. To see whether the factors that we identified in our model hold for biological membranes, we scaled the parameters of the model to typical biological dimensions. The model parameters, diffusion, barrier spacing, rate of barrier crossing, and rate of vesicle were assigned experimentally measured values.

The data for cell and vesicle dimensions and the vesicle trafficking rates were taken from Steinman et al. (1983), a quantitative measurement of endocytosis in L-cells. These data are: cell surface area = 2100 μm^2; cell diameter = 15 μm; vesicle surface area = 0.162 μm^2; vesicle diameter = 0.202 μm; internalization rate ~0.8%/min of surface area.

Note that the rate is measured in terms of total surface area internalized per unit time. Thus, the size of the vesicles is not expected to introduce any change in the results of the simulation. If the size of a vesicle is smaller, for instance, one will need more vesicles per unit time in order to achieve the same turnover time. Therefore, while the number of particles added or subtracted by a vesicle will be smaller, the time between successive such events will have to be shorter in order to preserve the total turnover time.

Diffusion coefficients for proteins were taken as $D \sim 10^{-9}$ cm^2/s (10^{-1} $\mu m^2/s$) for free diffusion, and $D \sim 10^{-10}$ cm^2/s (10^{-2} $\mu m^2/s$) for hindered diffusion (Edidin, 1987). We take the domain size as 0.5×0.5 μm^2, the order of magnitude for domains observed experimentally (summarized in the Introduction).

CALCULATION

We started by determining the units for time and length in our simulation. The domain size that we chose as 0.5×0.5 μm^2, based on experimental data, is larger than the diameter of one vesicle, so that the conditions of our unscaled simulation hold here; a vesicle delivers its contents to one domain, and not to several domains. Once this size is set, all other parameters are determined. The dimension of one pixel follows from that: 0.5 μm/8 pixels = 0.0625 μm/pixel (=62.5 nm/pixel). Because the array in the simulation has 128×128 pixels, it follows that the portion of cell we are watching is 8×8 μm^2 (64 μm^2).

The diffusion coefficient in 2D is $D = 1/4\ l^2/\tau$, and l, the step length from pixel to pixel, now is 0.0625 μm. Requiring this diffusion coefficient to be equal to the free diffusion coefficient $D = 10^{-1}$ $\mu m^2/s$ leads to:

$$D = (0.0625^2/4)\mu m^2/\tau = 0.1\ \mu m^2/s$$

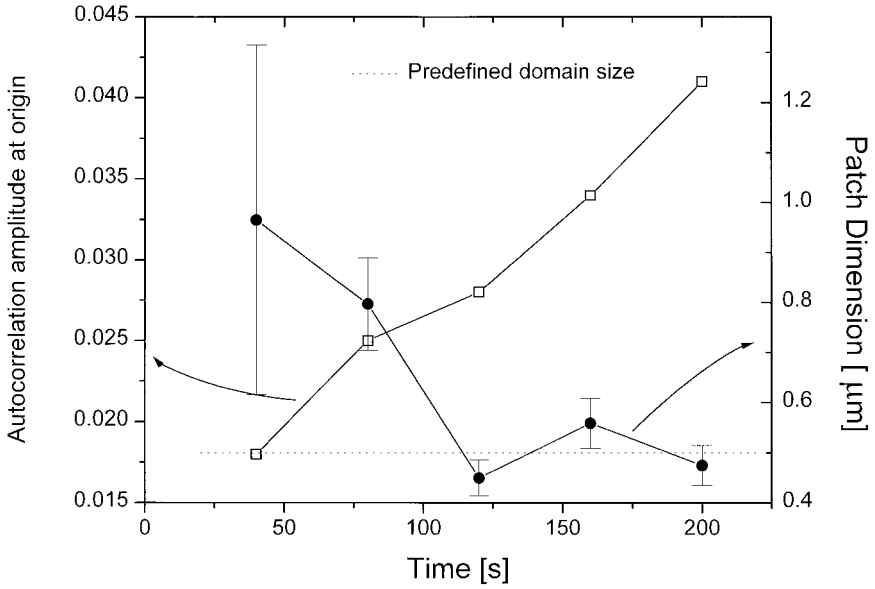

FIGURE 7 Summary of simulation with parameters scaled to real world. The simulation in this case is started with a random distribution with barriers to lateral diffusion and with vesicle traffic. The autocorrelation amplitude at the origin, reporting on the degree of clustering (*open squares*), is plotted with values on the left axis and increases constantly with time; the membrane becomes increasingly clustered. The size of the clusters (*filled circles*) is plotted with values on the right axis. It starts with a largely undefined cluster size 60 s after starting the simulation, but converges within 60 more seconds (at $t = 120$ s) to the predefined size of the domains (0.5 μm).

From this, the time unit is determined:

$$\tau = 0.01 \text{ s}.$$

This is the "real life" duration of one iteration of the simulation. From the data about the dimensions of cells and vesicles, we calculate the following:

$$A_c/A_v = 2100/0.162 \sim 13{,}000$$

where A_c is the surface area of cell and A_v is the surface area of vesicle. Thus, it takes 13,000 vesicles to replace the whole surface area of the cell, or $13{,}000 \times 0.008 = 104$ vesicles to replace 0.8% of the cell membrane. This occurs over 1 min, so in 1 s we have $104/60 \sim 1.73$ s^{-1}. That is, 1.73 vesicles fuse with the plasma membrane every second. However, we are watching only $64/2100 = 0.03$ of the whole surface area of the cell. Therefore, the number of vesicles fusing with the membrane in the observed area is $0.03 \times 1.73 = 0.05$ s^{-1}. A vesicle fuses with the membrane every ~20 s in the area observed, or once every 2000 iterations, because one iteration simulates 0.01 s. This sets the value for T_a and T_d to 2000.

The measured diffusion coefficient for obstructed diffusion is 0.01 μm^2/s. We performed a calculation similar to the one that led to determining the time represented by one iteration to determine the characteristic time to cross a barrier: 1 now is 0.5 μm and the equation is $D = 1/4\,(0.5^2)/T = 0.01$ μm^2/s. T is the characteristic time to cross from one domain to an adjacent one. From the equation one gets $T = 6.25$ s. This value is in excellent agreement with measured data (SPT) (Saxton and Jacobson, 1997). Because

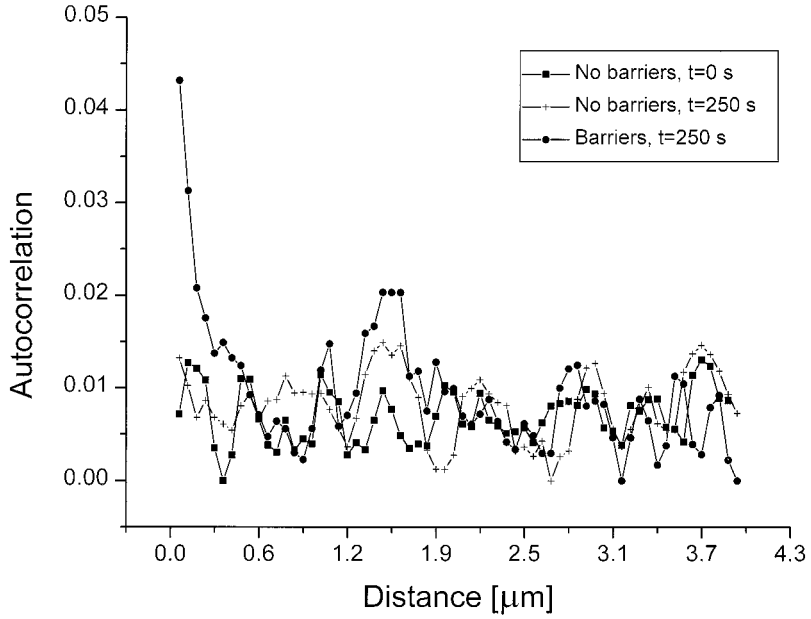

FIGURE 8 Comparison between a simulation with vesicle traffic only and a simulation with both vesicle traffic and barriers. Both simulations were run for 250 s ("cell" time), using the parameters calculated from the literature, as previously explained. For the simulation with vesicle traffic only, the autocorrelation did not show a difference between the start (*filled squares*) and the end (*crosses*) of the simulation. No clusters have formed under these conditions. As opposed, the autocorrelation for the barriers and vesicle traffic case clearly showed the presence of clusters after 250 s (*filled circles*). Vesicle traffic alone is not able of maintaining clusters.

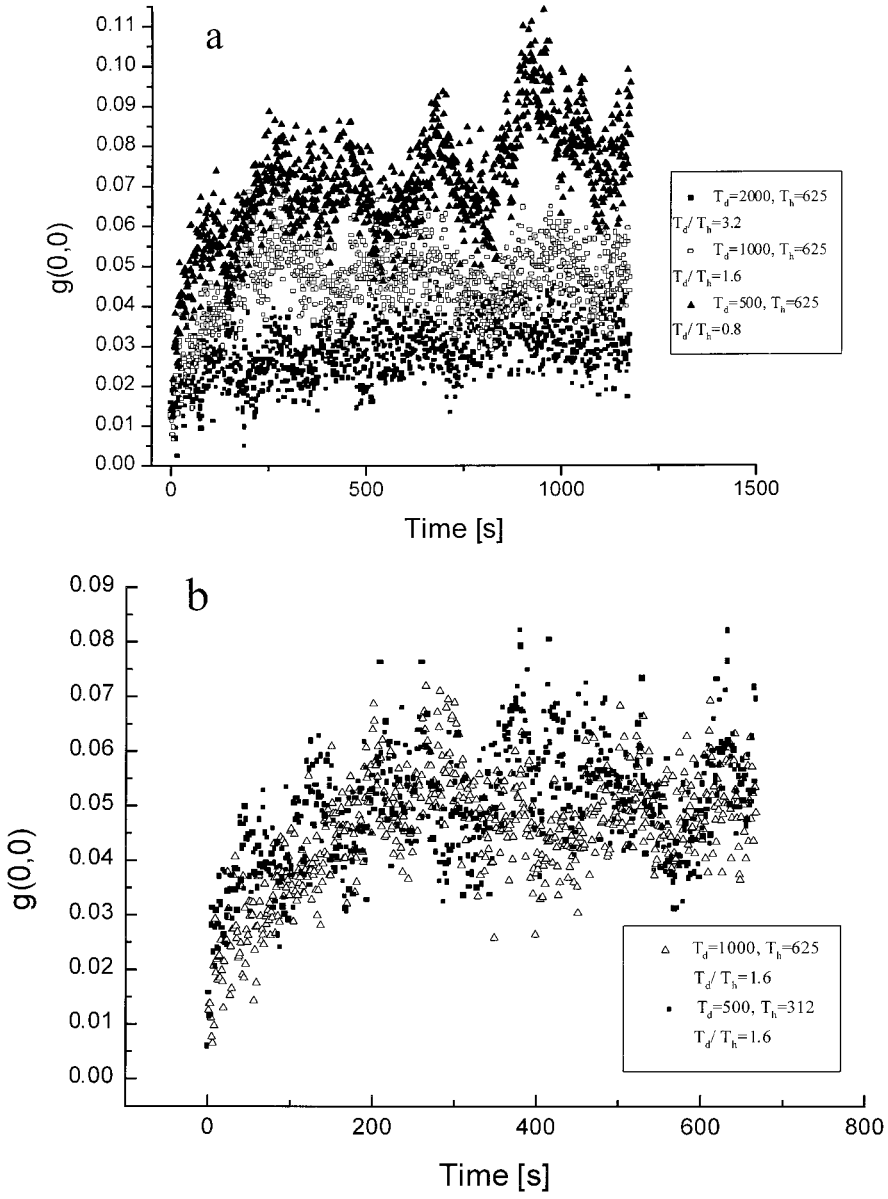

FIGURE 9 (*a*) The values of $g(0, 0)$, the autocorrelation value at the origin versus time for three different ratios T_d/T_h, as indicated in the inset. As the ratio T_d/T_h decreases, the value at which $g(0, 0)$ enters a plateau increases. The patchiness becomes more substantial as the dispersion of particles is slower in relation to the vesicle traffic rate. (*b*) Two plots of $g(0, 0)$ versus time for two different values of T_d and T_h giving the same T_d/T_h ratio (1.6), as indicated in the inset. The curves are practically identical. The ratio T_d/T_h is the important value, not the individual values of T_d and T_h.

one iteration in the simulation represents 0.01 s in real time, $T_h = 625$.

Finally, N, the number of particles added by an exocytic vesicle or removed by an endocytic vesicle, is assumed to be proportional to the ratio between the surface area of the vesicle and the surface area of one domain. Therefore, N is $0.162/0.25 = 0.65$, or 65% of the initial particle number in a domain. This calculation assumes that the concentration of particles in a vesicle is the same as that in the cell surface membrane. If the concentration of membrane proteins is higher in the vesicle than in the plasma membrane, the fusion of a vesicle will produce an even more concentrated, and hence persistent, patch than we observed.

The simulation is started with random distribution of particles, barriers, and delivery/intake. The goal is to check whether patches will form under these conditions, which simulate real conditions of a cell. The result is summarized in Fig. 7, which shows the magnitude of the autocorrelation function and the patch size as a function of time. The autocorrelation magnitude grew monotonically with time. The patch size converged to 0.5 μm within 120 s from the start and stayed constant for the rest of the simulation.

A similar simulation was performed, with identical parameters, except without barriers to lateral diffusion. The purpose of this simulation was to check whether the vesicle traffic alone can create and maintain patches. In Fig. 8 we compare the autocorrelation profiles at the beginning and the end of the simulation with no barriers, with that at the end of the simulation with barriers. The autocorrelation magnitude in the case with no barriers does not change over the time of the simulation and remains flat, indicating a random distribution of particles.

Influence of the various parameters

The most important criterion in determining whether clusters will form is the ratio of the characteristic time for vesicle traffic, $T_{a,d}$, to the characteristic time for crossing a barrier, T_h. $T_{a,d}/T_h$ defines at what rate concentration variations are replenished, in relation with the rate at which these local variations are being "cleared" across barriers. The larger this ratio is, the less likely clusters are likely to appear, because it means that the local concentrations are rapidly dispersed across barriers.

To show that this is the case, we present the results of long simulations, with different $T_{a,d}/T_h$ ratios, where all other parameters were held constant and identical to the simulation described above. The autocorrelation was calculated every second (100 iterations). In Fig. 9 *a* we plot the value of $g(0, 0)$ as a function of time for three different cases, as shown in the figure. $T_d = 2000$, $T_h = 625$ is the simulation discussed above, representing a typical L-cell, the other two are simulations with faster trafficking rates (shorter periods between events). It is readily observed that decreasing the ratio $T_{a,d}/T_h$ increases the value of $g(0, 0)$ at the plateau reached after ~5 min (~300 s). In order to show that the ratio is the important parameter, and not the actual values of $T_{a,d}$ or T_h, in Fig. 9 *b* we plot a pair of similar curves for similar ratios, each having different values of $T_{a,d}$ and T_h. The curves are basically identical.

It is important to mention that the set of parameters for which the first simulation was performed constitute the "worst case" scenario for clusters to appear. This is so because the assumptions of the algorithm were such that they decreased the probability of clusters forming. One such assumption is that the concentration of particles in an arriving vesicle is the same as the concentration of the particles on the plasma membrane. This is usually not the case, because vesicles contain higher concentrations of specific proteins. Such an assumption will lead to larger values for $N_{a,d}$, and the variation of concentration within one compartment would be larger, leading to a higher patchiness. The turnover time of the membrane assumed is a relatively low one. Turnover times can be as short as 30 min for some species of phagocytes. A faster turnover time means a faster rate of delivery/intake, so $T_{a,d}$ would be considerably smaller, while T_h would not change. This will decrease the T_d/T_h ratio and will consequently increase the patchiness.

We also addressed the assumption that the delivery/intake occurs with equal probability all over the membrane. If one assumes that both exocytosis and endocytosis occur at a specific, nonrandom set of points on the plasma membrane, but this set of points is the same for both processes, the results are identical to the homogenous distribution case. However, a more realistic assumption would be that exocytosis occurs at such a set of constant points, while endocytosis occurs with equal probability at any point. In such a case, the patchiness increases considerably. One result of such a simulation is plotted in Fig. 10. The delivery was limited to only 25% of the existent sites on the membrane, while the intake was allowed to occur from any site. All other parameters were identical to the original simulation. It can be seen that the nonrandom case gives rise to higher patchiness that does not seem to enter a plateau even after 1000 s.

Lifetime of patches

We followed the evolution with time of individual compartments delineated by dynamic barriers. In Fig. 11 we plot the population (the sum of all values of pixels in the compartment) of two different compartments as a function of time,

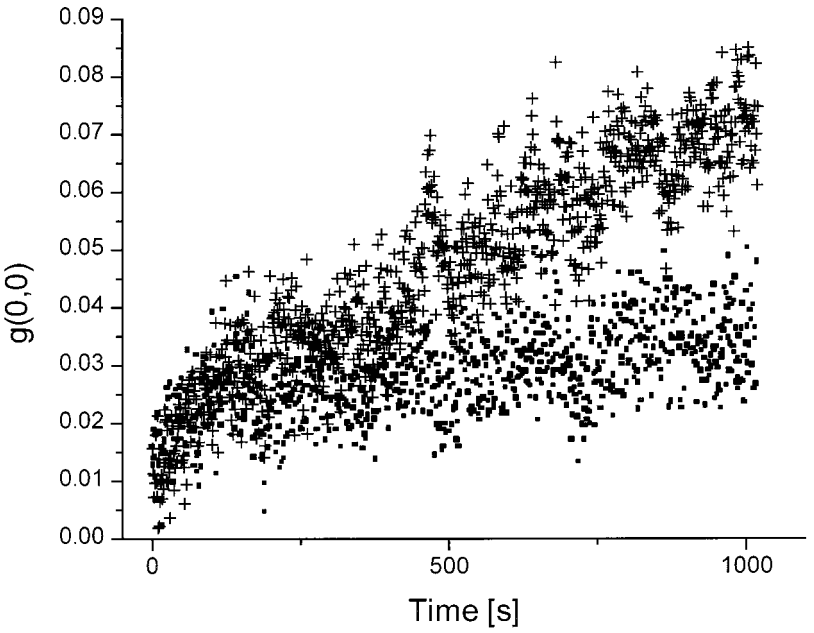

FIGURE 10 Comparison of $g(0, 0)$ versus time for two cases: homogenous distribution of delivery and intake sites (*solid squares*), and delivery limited to only 25% of the sites and intake from all the available sites (*crosses*). The values of all the parameters are identical for both cases and identical to the simulation summarized in Fig. 7. The curve for the limited number of sites increases continuously and does not enter a plateau even after 1,000 s. The patchiness for such a case is considerably higher than for the case with homogenous distribution of exocytosis sites.

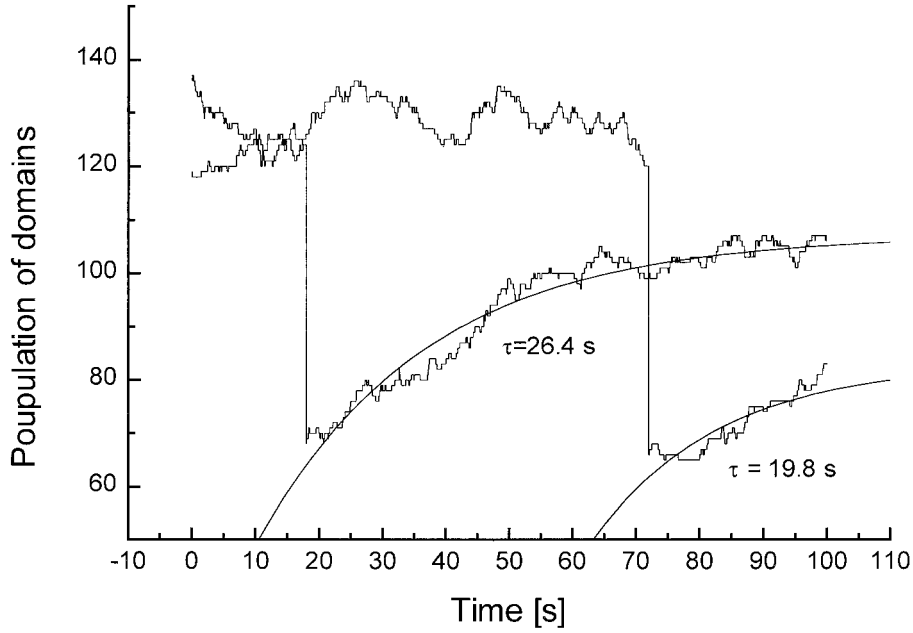

FIGURE 11 The dynamics of single compartments. The population (total number of particles) of two different compartments is plotted as a function of time. Both compartments undergo an endocytosis event, the first around $t = 20$ s and the second around $t = 70$ s. After the sudden decrease in the population, both compartments show a gradual increase in the number of particles due to diffusion of particles from adjacent compartments (across barriers). This trend is fitted with a function of the form $Y = A - (B \exp(-(t - t_0)/\tau))$, also plotted in the figure. The characteristic lifetime, $\tau = 26.4$ and $\tau = 19.8$, is shown in the figure for each of the curves.

as an example. The plot in Fig. 11 describes the history of two compartments from which endocytosis had occurred at some point in time. After the instant decrease in the number of particles, representing the intake event, the compartments' population is rising slowly, due to diffusion of particles from neighboring compartments, across barriers, into the depleted compartment. This raise was fitted to a function of the form $Y = A - (B \exp(-(t - t_0)/\tau))$, which is also plotted in the figure. The best fit yields a characteristic lifetime (τ) of ~20 s, with an asymptote (A) of 124 particles for very long times, which is similar to the initial population of the compartment before the endocytosis event. Results for compartments that underwent an exocytosis event were identical. These results were obtained from the simulation with the original choice of parameters, representing an L-cell. We note that within these patches, whose dimensions and geometry are determined by the dynamic barriers, there may appear smaller domains, with a much shorter lifetime (100-fold shorter), such as those described in Abney and Scalettar (1995). Such domains may appear as a result of fluctuations in particle density, however, being so short-lived and small (~100 nm), on the background of the large and long-lived domains formed by the mechanism we model, their detection is practically impossible.

CONCLUSIONS

A model of the cell surface that combines lateral diffusion hindered by barriers with vesicle traffic creates and maintains patches of membrane proteins and lipids whose sizes are similar to the size of the membrane domains inferred from a variety of experiments. Though an individual patch produced in this way has a short lifetime compared with the cell lifetime, the population of patches is maintained by vesicle traffic. Our results with the model suggest that although membrane domains may arise due to specific molecular associations, much of the lateral heterogeneity detected in any membrane, particularly that observed by microscopy, may be nonspecific. Though our model makes no assumptions about the diffusing species, it is most appropriate to transmembrane proteins. We expect that the lateral diffusion of membrane lipids will not be confined by the submembrane barriers that we use in the model. Hence, newly delivered lipid molecules ought to diffuse rapidly from the point of their insertion into the plasma membrane. The rate of their dispersion would of course be affected by their interactions with membrane proteins. Similarly, we expect that the dispersion of GPI-anchored proteins will be slower than that of lipids, to the extent that these proteins can interact, through their exodomains, with transmembrane proteins. We also note that weak associations of membrane molecules, for example lipid phase separations (Brown and London, 1997) will be quickly disrupted by vesicle traffic. Finally, we predict that disrupting vesicle traffic at the cell surface, for example by overexpressing dominant negative mutants of proteins required for endocytosis (Damke et al., 1995) will initially increase the size of patches and at the same time reduce the concentrations of proteins and lipids in patches relative to the average for an entire membrane.

This work was supported by National Institutes of Health grants AI 14584 and GM 58554 (to M.E.).

REFERENCES

Abney, J. R., and B. A. Scalettar. 1995. Fluctuations and membrane heterogeneity. *Biophys. Chem.* 57:27–36.

Betzig, E., and J. Trautman. 1992. Near-field optics: microscopy, spectroscopy, and surface modification beyond the diffraction limit. *Science.* 257:189–195.

Betzig, E., J. Trautman, T. D. Harris, J. S. Weiner, and R. L. Kostelak. 1991. Breaking the diffraction barrier: optical microscopy on a nanometric scale. *Science.* 251:1468–1470.

Brown, D. A., and E. London. 1997. Structure of detergent-resistant membrane domains: does phase separation occur in biological membranes? *Biochem. Biophys. Res. Commun.* 240:1–7.

Damjanovich, S., R. J. Gaspar, and C. Pieri. 1997. Dynamic receptor superstructures at the plasma membrane. *Q. Rev. Biophys.* 30:67–106.

Damke, H., T. Baba, A. M. van der Bliek, and S. L. Schmid. 1995. Clathrin-independent pinocytosis is induced in cells overexpressing a temperature-sensitive mutant of dynamin. *J. Cell. Biol.* 131:69–80.

Denisov, G., S. Wanaski, P. Luan, M. Glaser, and S. McLaughlin. 1998. Binding of basic peptides to membranes produces lateral domains enriched in the acidic lipids phosphatidylserine and phosphatidylinositol 4,5-bisphosphate: an electrostatic model and experimental results. *Biophys. J.* 74:731–744.

Edidin, M. 1992. Patches, posts and fences: proteins and plasma membrane domains. *Trends Cell Biol.* 2:376–380.

Edidin, M. 1987. Rotational and lateral diffusion of membrane proteins and lipids: phenomena and function. *Curr. Topics Membr. Transport.* 29: 91–127.

Edidin, M. 1997. Lipid microdomains in cell surface membranes. *Curr. Opin. Struct. Biol.* 7:528–532.

Edidin, M., S. C. Kuo, and M. Sheetz. 1991. Lateral movements of membrane glycoproteins restricted by dynamic cytoplasmic barriers. *Science.* 254:1379–1382.

Edidin, M., and I. Stroynowski. 1991. Differences between the lateral organization of conventional and inositol phospholipid-anchored membrane proteins. A further definition of micrometer scale membrane domains. *J. Cell Biol.* 112:1143–1150.

Edidin, M., M. C. Zuniga, and M. P. Sheetz. 1994. Truncation mutants define and locate cytoplasmic barriers to lateral mobility of membrane glycoproteins. *Proc. Natl. Acad. Sci. USA.* 91:3378–3382.

Feder, T. J., W. W. Webb, B. Baird, J. P. Slattery, and I. Brust-Mascher. 1996. Constrained diffusion or immobile fraction on cell surfaces: a new interpretation. *Biophys. J.* 70:2767–2773.

Gheber, L. A., J. Hwang, and M. Edidin. 1998. Design and optimization of a near-field scanning optical microscope for imaging biological samples in liquid. *Appl. Opt.* 37:3574–3581.

Holowka, D., and B. Baird. 1996. Antigen-mediated IGE receptor aggregation and signaling: a window on cell surface structure and dynamics. *Annu. Rev. Biophys. Biomol. Struct.* 25:79–112.

Hwang, J., L. A. Gheber, L. Margolis, and M. Edidin. 1998. Domains in cell plasma membranes investigated by near-field scanning optical microscopy. *Biophys. J.* 74:2184–2190.

Jain, M. K., and H. White. 1977. Long range order in biomembranes. *Adv. Lipid Res.* 15:1–60.

Kusumi, A., and Y. Sako. 1996. Cell surface organization by the membrane skeleton. *Curr. Opin. Cell Biol.* 8:566–574.

Monks, C. R. F., B. A. Freiberg, H. Kupfer, N. Sciaky, and A. Kupfer. 1998. Three-dimensional segregation of supramolecular activation clusters in T cells. *Nature.* 395:82–86.

Peters, R. 1988. Lateral mobility of proteins and lipids in the red cell membrane and the activation of adenylate cyclase by beta-adrenergic receptors. *FEBS Lett.* 234:1–7.

Piknova, B., D. Marsh, and T. E. Thompson. 1996. Fluorescence-quenching study of percolation and compartmentalization in two-phase lipid bilayers. *Biophys. J.* 71:892–897.

Pralle, A., E.-L. Florin, E. H. K. Stelzer, and J. K. H. Hörber. 1999. Localized diffusion measurements by 3D-SPT provide support for membrane microdomains. *Biophys. J.* 76:390*a*. (Abstr.).

Sabra, M. C., and O. G. Mouritsen. 1998. Steady-state compartmentalization of lipid membranes by active proteins. *Biophys. J.* 74:745–752.

Sako, Y., and A. Kusumi. 1995. Barriers for lateral diffusion of transferrin receptor in the plasma membrane as characterized by receptor dragging by laser tweezers: fence versus tether. *J. Cell Biol.* 129:1559–1574.

Saxton, M. J., and K. Jacobson. 1997. Single-particle tracking: applications to membrane dynamics. *Annu. Rev. Biophys. Biomol. Struct.* 26: 373–399.

Scheiffele, P., M. G. Roth, and K. Simons. 1997. Interaction of influenza virus hemagglutinin with sphingolipid-cholesterol membrane domains via its transmembrane domain. *EMBO J.* 16:5501–5508.

Schnapp, B. J., J. Gelles, and M. P. Sheetz. 1988. Nanometer-scale measurements using video light microscopy. *Cell Motil. Cytoskeleton.* 10: 47–53.

Sheets, E. D., K. Jacobson, R. Simson, and G. M. Lee. 1997. Transient confinement of a glycosylphosphatidylinositol-anchored protein in the plasma membrane. *Biochemistry.* 36:12449–12458.

Simons, K., and E. Ikonen. 1997. Functional rafts in cell membranes. *Nature.* 387:569–572.

Singer, S. J., and G. L. Nicolson. 1971. The fluid mosaic model of the structure of cell membranes. *Science.* 175:720–731.

Stauffer, T. P., and T. Meyer. 1997. Compartmentalized IgE receptor-mediated signal transduction in living cells. *J. Cell Biol.* 139:1447–1454.

Steinman, R. M., I. S. Mellman, W. A. Muller, and Z. A. Cohn. 1983. Endocytosis and the recycling of plasma membrane. *J. Cell Biol.* 96: 1–27.

Thompson, T. E., M. B. Sankaram, R. L. Biltonen, D. Marsh, and W. C. L. Vaz. 1995. Effects of domain structure on in-plane reactions and interactions. *Molec. Membr. Biol.* 12:157–162.

Tomishige, M., and A. Kusumi. 1998. Regulation of lateral movements of erythrocyte band 3 by membrane skeleton as studied by single particle tracking and optical tweezers. *Biophys. J.* 74:223 *a*. (Abstr.).

Yechiel, E., and M. Edidin. 1987. Micrometer scale domains in fibroblast plasma membranes. *J. Cell Biol.* 105:755–760.